Supporting Information

Zhang et al. 10.1073/pnas.1406233111

SI Materials and Methods

Materials. Common reagents were purchased from Sigma-Aldrich and used as received unless otherwise specified. 2,2′-Azobis(2,4-dimethylvaleronitrile) (V-65), 2,2′-azobis[2-(2-imidazolin-2-yl) propane]dihydrochloride (VA-044) were from Wako; 4,4-azobis (4-cyanopentanoic acid) (V-501) was from Fisher Scientific. *N,N′*-Dicyclohexylcarbodiimide (DCC) and 4-(dimethylamino) pyridine (DMAP) were obtained from AAPPTEC. Paclitaxel (PTX, >99.5%) was purchased from LC Laboratories. Gemcitabine hydrochloride (GEM, ≥99.0%) was purchased from NetQem LLC. Iodine-125 [^{125}I] was obtained from Perkin-Elmer. $^{111}InCl_3$ was from Intermountain Radiopharmacy. 1-Hydroxybenzotriazole (HOBt) and *N*-Boc-ethylenediamine were purchased from AnaSpec. Cyanine5 amine (Cy5 amine) was purchased from Lumiprobe. *p*-SCN-Bn-DTPA was purchased from Macrocyclics. Reversible addition-fragmentation chain transfer (RAFT) agents, 4-cyanopentanoic acid dithiobenzoate (1), and peptide2CTA (*N,N*'-bis(4-cyano-4-(phenylcarbonothioylthio)pentanoylglycylphenylalanylleucylglycyl)lysine) (2) were synthesized according to the literature.

Synthesis of Monomers. *N*-(2-Hydroxypropyl)methacrylamide (HPMA) was synthesized by acylating 1-aminopropan-2-ol with methacryloyl chloride in acetonitrile, as previously described (3). Melting point: 69–71 °C; *N*-methacryloylglycylphenylalanylleucylglycine (MA-GFLG-OH) (4), *N*-methacryloyltyrosinamide (MA-Tyr-NH_2) (5), *N*-methacryloylaminopropyl fluorescein thiourea (MA-FITC) (6), and 3-(*N*-methacryloylglycylphenylalanylleucylglycyl)thiazolidine-2-thione (MA-GFLG-TT) (7) were synthesized as previously described.

Polymerizable drug derivatives. *N*-Methacryloylglycylphenylalanylleucylglycyl)paclitaxel (MA-GFLG-PTX) was prepared by the reaction of MA-GFLG-OH with paclitaxel in DMF in the presence of DCC using DMAP as catalyst according to reported procedure (8). *N*-Methacryloylglycylphenylalanylleucylglycyl)gemcitabine (MA-GFLG-GEM) was prepared by the reaction of MA-GFLG-TT with gemcitabine hydrochloride in pyridine at 50 °C (9).

Synthesis of 2-(N-methacryloylglycylphenylalanylleucylglycine)-N′-Boc-ethylenediamine (MA-GFLG-NH-Boc). MA-GFLG-OH (1.38 g, 3 mmol), *N*-Boc-ethylenediamine (0.48 g, 3 mmol), HOBt (405 mg, 3 mmol), and DIPEA (1.05 mL, 6 mmol) were dissolved in 6 mL of DMF and cooled to 0 °C. HBTU (1.14 g, 3 mmol) in 0.5 mL of DMF was added dropwise to the solution. The reaction mixture was stirred at 0 °C for 1 h then left at room temperature overnight. DMF was evaporated at reduced pressure. Ethyl acetate was added, and the organic solution was washed sequentially with 3 × 20 mL of 5% (wt/vol) aq. $NaHCO_3$, 3 ×20 mL of 1 N citric acid, and 3 × 20 mL of aq. NaCl, then dried over anhydrous $MgSO_4$. The solvent was evaporated at reduced pressure. The product was recrystallized from ethyl acetate/ether. Yield 0.96 g (53.3%, white powder). The product was confirmed by MALDI ToF Mass: $[M+Na]^+$ 625, $[M+K]^+$ 641 (Fig. S1).

Synthesis of Diblock-Degradable HPMA Copolymer Drug Conjugates.

Synthesis of diblock-degradable HPMA copolymer-gemcitabine conjugates (2P-GEM/2P-GEM-Tyr). The synthesis of second-generation HPMA-copolymer gemcitabine conjugate was similar to that previously described (10). Briefly, an ampoule containing MA-GFLG-GEM (63.5 mg, 0.09 mmol) was attached to the Schlenk-line. After three vacuum-nitrogen cycles to remove oxygen, 0.15 mL degassed DMSO acidified with 5 μL acetic acid was added and a clear colorless solution was obtained. A degassed HPMA aqueous solution (130 mg, 0.91 mmol in 0.3 mL DI H_2O) was added into the ampoule via syringe under vigorous stirring. Following addition of RAFT agent peptide2CTA and initiator V-501, the ampoule was sealed, and copolymerization was performed at 70 °C for 16 h. The polymer was obtained by precipitation into acetone and purified by redissolving in methanol and precipitation in acetone two more times. The copolymer was isolated as a light pink powder and dried under vacuum. Yield: 110 mg (60%).

The average molecular weight (Mw) and the polydispersity of the conjugates were determined by size-exclusion chromatography (SEC) on an AKTA FPLC system equipped with a UV detector (GE Healthcare), miniDAWN TREOS, and OptilabrEX (refractive index) detector (Wyatt Technology) using a Superose 6 HR10/30 column with sodium acetate buffer containing 30% (vol/vol) acetonitrile (pH 6.5) as mobile phase. HPMA homopolymer fractions were used as molecular weight standards. The characterization of conjugates is summarized in Table S1.

The product (100 mg) was further reacted with V-65 (10 mg, 0.036 mmol, over 40-times excess with respect to the polymer end groups) in 1 mL MeOH at 50 °C for 2 h, purified by precipitation into acetone twice, resulting in diblock degradable HPMA copolymer-GEM conjugate (2P-GEM).

To synthesize a radioactively labeled diblock conjugate, comonomer MA-Tyr-NH_2 (3.7 mg, 0.015 mmol) was added into ampoule and the procedure shown above used.

Synthesis of diblock degradable HPMA copolymer-paclitaxel conjugates (2P-PTX/2P-PTX-Tyr). The RAFT copolymerization was accomplished in methanol at 50 °C for 24 h using Peptide2CTA as chain transfer agent and V65 as initiator as previously reported (8). For example, HPMA (275 mg, 1.92 mmol), MA-GFLG-PTX (80 mg, 0.06 mmol), and MA-Tyr-NH_2 (7.5 mg, 0.03 mmol) were added into an ampoule. After three vacuum-nitrogen cycles, 1 mL methanol was added to the ampoule followed by addition of Peptide2CTA and initiator V-65 via syringe. The solution was then kept in ice bath and bubbled with N_2 for 30 min. The ampoule was sealed and kept stirring in an oil bath. The copolymer was precipitated in acetone, isolated by centrifugation, and purified by dissolution-precipitation in methanol-acetone twice, then dried under vacuum at room temperature. The copolymer was obtained as a slightly pink powder with yield 186 mg (51.4%).

The removal of end-dithiobenzoate group was conducted by postpolymerization modification. The solution in methanol containing conjugate (180 mg) and V65 (18 mg, over 40 times excess with respect to the polymer end groups) was kept at 50 °C for 2 h and then isolated by precipitation into acetone.

Synthesis of Traditional (First-Generation) HPMA Copolymer-Drug Conjugates. To enable comparison of the activity of second-generation HPMA copolymer-drug conjugates (2P-GEM and 2P-PTX) to that of first-generation HPMA copolymer-drug conjugates (P-GEM and P-PTX with Mw < 50 kDa), the copolymerization of HPMA with MA-GFLG-GEM or MA-GFLG-PTX was conducted as described above but using 4-cyanopentanoic acid dithiobenzoate (CPA) as the chain transfer agent. In a typical copolymerization for the synthesis of P-PTX, HPMA (275 mg, 1.92 mmol) and MA-GFLG-PTX (104 mg, 0.08 mmol) were dissolved in methanol under N_2 atmosphere. CPA and V-65 at a molar ratio of 4:1 were added through syringe. The ampoule was sealed and the polymerization was carried out at 50 °C for 24 h. The copolymer was precipitated in acetone, washed with acetone three times, and dried under reduced

pressure at room temperature. The dithiobenzoate end group was removed by radical-induced modification with excess of V-65. Yield was 190 mg white powder (50%.)

Synthesis of Dual-Radioisotope–Labeled Model Conjugate ^{125}I-Tyr-P-DTPA-^{111}In. The synthetic scheme is shown in Fig. 1*C*. As chelating agent of ^{111}In, DTPA was selected as a model drug that was conjugated to HPMA polymer backbone via enzyme-cleavable tetrapeptide GFLG linker. MA-GFLG-NH-Boc was synthesized first as described above. The polymer precursors (first generation and second generation) were obtained by RAFT copolymerization of HPMA (130 mg), MA-Tyr-NH_2 (4 mg), and MA-GFLG-NH-Boc (35 mg) following the procedure of synthesis of GEM conjugate in H_2O/DMSO at 70 °C using V-501 as initiator, CPA and Peptide2CTA as RAFT agents, respectively.

After end-modification, the polymer precursor (76 mg) was dissolved in 0.5 mL of distilled water followed by addition of 1 mL trifluoroacetic acid. The sample was kept stirring in ice-bath for 30 min, then condensed under reduced pressure and precipitated in precooled ether/acetone. The polymer was isolated by centrifugation and dried under N_2 flow, then purified by dissolution/precipitation. The polymer was analyzed by ninhydrin assay (11) to determine side-chain amino content ([NH_2] = 133 nmol/mg polymer).

Coupling of *p*-SCN-Bn-DTPA was accomplished according to the procedure described in the literature (12). Briefly, 24 mg polymer precursor was dissolved in 250 μL 0.2 N $NaHCO_3$ containing 10 mM EDTA (pH 8.5), then mixed with 10× excess of p-SCN-Bn-DTPA (20 mg, 31 μmol) in 100 μL DMSO. After stirring 5 h at room temperature, the volume of the sample was adjusted to 500 μL with deionized (DI) H_2O. The sample was applied to a pre-equilibrated PD-10 Sephadex G25 column (GE Healthcare) with DI H_2O for primary purification. The fraction of 2.5–4.5 mL was collected and was further purified by ultracentrifugation using 3000 Da cutoff membrane and washed with DI H_2O three times. The final sample in DI H_2O was freeze-dried to give white flurry polymer-DTPA model conjugate. In this section, high-purity deionized H_2O was used.

The DTPA content was determined using spectrophotometric method developed by Pippin et al. (13). This method is based on the reaction between DTPA and an yttrium (III) complex of araenazo III:

$$\mathrm{Y(AAIII)_2 + DTPA = Y(DTPA) + 2AAIII}$$

The complex of AAIII and Y(III) has a feature absorbance at 652 nm. Titration of the complex with DTPA resulted in the decrease of the absorbance at 652 nm. The changes obeyed Beer's law in a certain range of DTPA. Thus, a calibration curve can be recorded and consequently, the DTPA content in the polymer can be calculated. For example, the complex $Y(AAIII)_2$ was first prepared by mixing of 30 μL 10 mM AAIII in 0.15 N sodium acetate buffer (pH 4.0) with 0.96 mL 0.1 mM Y(III), and the volume was adjusted to 20 mL. The absorbance of the complex at 652 nm was measured. A series of standard solutions was prepared by adding a variable volume of 0.1 mM DTPA solution to the complex while keeping total volume constant. A calibration curve was obtained by measuring the absorbance of standard solutions at 652 nm. The content of DTPA in polymer conjugate Tyr-P-DTPA was then calculated as 74 nmol/mg polymer. The conversion was 55.6%.

Radiolabeling. ^{125}I labeling of polymer pendant tyrosinamide moieties and ^{111}In labeling of DTPA (bound via a cleavable GFLG spacer) were conducted immediately before use. For single labeling of ^{125}I, HPMA copolymer-drug conjugates (P-PTX, P-GEM, 2P-PTX and 2P-GEM), containing tyrosinamide in the side chains, were reacted with Na^{125}I (Perkin-Elmer) at room temperature in 0.01 M phosphate buffer containing chloramine-T for 30 min and then purified with Sephadex PD-10 columns (GE Healthcare). The specific activity of the hot samples was in the range 50–80 μCi/mg. For dual-labeling of ^{111}In/^{125}I, model conjugate Tyr-P-DTPA was first reacted with Na^{125}I (Perkin-Elmer) at room temperature in 0.01 M phosphate buffer containing chloramine-T for 30 min and then purified with ultrafiltration tube (Millipore) to remove chloramine-T. After purification, ^{125}I-Tyr-P-DTPA in 0.1 M sodium acetate solution (pH 5.2) was mixed with an aqueous solution of $^{111}InCl_3$ at room temperature for 30 min and then purified with Sephadex PD-10 columns (GE Healthcare) to produce ^{125}I-Tyr-P-DTPA-^{111}In.

Synthesis of Dual-Fluorophore–Labeled Model Conjugates FITC-P-Cy5. In this model conjugate, FITC was covalently attached to polymer backbone by copolymerization of HPMA with polymerizable FITC derivative, *N*-methacryloylaminopropyl fluorescein thiourea (MA-FITC) (6). Thus, the observed images of FITC detect polymer backbone. Consequently, Cy5 was conjugated to polymer chains via a cleavable GFLG linker as a model drug. We designed to use MA-GFLG-TT for RAFT copolymerization with HPMA and MA-FITC to incorporate pendant GFLG-TT moieties. Next, the amino-active group, TT was aminolyzed by Cy5 amine to give FITC-P-Cy5 model conjugate. The synthetic approach is shown in Fig. 1*D*.

RAFT copolymerization was carried out in methanol at 40 °C using CPA as chain transfer agent and VA-044 as initiator. After 24-h polymerization, the polymer was precipitated in ether/acetone and isolated by filtration. The polymer was purified by redissolving in methanol followed by reprecipitation in acetone twice, and dried under N_2. The product was characterized by Mw and Mw/Mn using AKTA system as described above. The contents of FITC and TT in polymer precursor FITC-P-TT were estimated by UV-vis spectrophotometry, using molar extinction coefficient ε_{495} = 82,000 $M^{-1}\cdot cm^{-1}$ in 0.1 M sodium borate buffer (pH 9.0) for FITC (6) and ε_{305} = 9,000 $M^{-1}\cdot cm^{-1}$ in methanol for TT (7), respectively.

Incorporation of Cy5 to side-chain of HPMA copolymer via GFLG linker was realized by reaction of Cy5 amine with FITC-P-TT in methanol (2:1 ratio of Cy5-NH_2 to TT groups). The polymer was applied to PD-10 column for separation of free Cy5 from polymer model conjugate. The final FITC-P-Cy5 was obtained after freeze-drying.

In Vitro Degradation of Conjugates (2P-PTX, 2P-GEM) and Release of Drugs (PTX, GEM) from Conjugates. The degradability of conjugates (2P-PTX, 2P-GEM) and the release of drugs (PTX, GEM) from the polymer conjugates were investigated by incubation of the conjugates in McIlvaine's buffer (50 mM citrate/0.1 M phosphate; 2 mM EDTA, pH 6.0) at 37 °C in the presence of papain (2.0 μM) with concentration of polymer 3 mg/mL for 12 h. At predetermined time points, a sample was withdrawn and analyzed by HPLC (Agilent Technologies) for drug release and by SEC (GE Healthcare) for backbone degradation. All degradation and cleavage determinations were carried out in duplicate.

Cell Culture. A2780 human ovarian cancer cells (ATCC) were maintained at 37 °C in a humidified atmosphere containing 5% CO_2 in RPMI-1640 medium (Gibco) supplemented with 10% FBS and a mixture of antibiotics (100 units/mL penicillin, 0.1 mg/mL streptomycin).

In Vitro Cytotoxicity Study. The cytotoxicity of free drugs (PTX, GEM) and their polymeric conjugates (2P-PTX, 2P-GEM) against A2780 human ovarian cancer cells was measured by CCK-8 assay (Dojindo). The cells were seeded in 96-well plates at the density of 10,000 cells per well in RMPI-1640 media containing 10% FBS. After 24 h, media was replaced and media containing

the drugs was added. The cells were incubated with free drugs (PTX, GEM) or their polymeric conjugates (2P-PTX, 2P-GEM) at a series of drug concentrations. After 24 h of incubation, the medium with drugs was removed and replaced with fresh medium without drugs. After 48 h, the number of viable cells was estimated using CCK-8 kit according to the manufacturer's protocol. In brief, medium was discarded and replaced with 100 μL fresh growth medium in each well, followed by the addition of 50 μL 5× diluted CCK-8 solution. Dehydrogenase activities in live cells converted the water-soluble tetrazolium salt WST-8 into a soluble yellow-color formazan dye. After the incubation of cells at 37 °C, 5% CO_2 for 2 h, the absorbance was measured using a microplate reader at 450 nm (630 nm as reference). Untreated control cells were set as 100% viable.

Combination Effect Analysis: Chou–Talalay's Method. Synergism, additivity, or antagonism of the combination was determined by the Chou–Talalay method (14, 15). As shown in Table S2, A2780 cells were treated with different sequential combination at a constant molar ratio (PTX: GEM = 1:1) using drug-concentration close to IC_{50} values of PTX and GEM. A combination index (CI) was determined with the following equation: $CI = (D)_1/(Dx)_1 + (D)_2/(Dx)_2 + \alpha(D)_1(D)_2/(Dx)_1(Dx)_2$, where $(Dx)_1$ is the dose of agent 1 required to produce x percent effect alone, and $(D)_1$ is the dose of agent 1 required to produce the same x percent effect in combination with $(D)_2$. Similarly, $(Dx)_2$ is the dose of agent 2 required to produce x percent effect alone, and $(D)_2$ is the dose required to produce the same effect in combination with $(D)_1$. Different values of CI may be obtained by solving the equation for different values of fraction affected (Fa; e.g., different degrees of cell growth inhibition). Here, CI values are plotted against drug effect level Fa. CI values of <0.9 indicate synergy (the smaller the value, the greater the degree of synergy), values >1.1 indicate antagonism and values between 0.9 and 1.1 indicate additive effects. Each experiment was carried out with triplicate cultures for each data and was repeated independently at least three times. The CI values are summarized in Table S3.

Cell Cycle Analysis. A2780 cells (2×10^5 cells per 2 mL) were seeded in six-well plates, and treated with drug alone, conjugate alone, or different sequential combinations shown in Table S2. Following treatment, cells were harvested, fixed and stained with propidium iodide at room temperature in the dark. Cell cycle analysis was performed by flow cytometry using BD LSR Fortessa machine (BD Biosciences). Cell percentages in the different phases of cell cycle were analyzed using FlowJo software (Tree star).

Annexin V/7-AAD Assay. A2780 cells were seeded in six-well plates at the concentration of 2×10^5 cells per well and then incubated for 24 h before treatment. Following treatments shown in Table S2 (PTX = 10 nM, GEM = 10 nM, 2P-PTX = 20 nM, and 2P-GEM = 20 nM), cells were harvested, fixed and stained with FITC-Annexin V and 7-AAD (7-aminoactinomycin D) using a commercial kit (Biolegend) according to the manufacturer's instructions. Cell analysis was performed by flow cytometry using BD LSR Fortessa machine (BD Biosciences). Cell percentages were analyzed using FlowJo software.

Cell Migration/Invasion Assay. A2780 cells were seeded in six-well plates at 2×10^5 cells per well in 2 mL complete growth media. After 24 h, the cells received treatments as described in Table S2 (PTX: 10 nM, GEM: 10 nM, 2P-PTX: 20 nM, and 2P-GEM: 20 nM). After treatment, the cells were starved with RPMI-1640 medium without FBS for 24 h. After 24-h serum starvation, cells were trypsinized, neutralized with PBS plus 5% (wt/vol) BSA, and resuspended in FBS-free RPMI-1640 medium. Cell migration/invasion assay was performed using Cultrex 8 μm Boyden chambers (Trevigen). For the invasion assay, the top chamber was previously coated with 50 μL 0.1× basement membrane extract on ice and was then allowed to polymerize at 37 °C overnight. Typically, cells (2×10^5 cells/50 μL) were added to the top of each migration/invasion chamber and were allowed to migrate to the underside of the chamber for 48 h in the presence of RMPI-1640 medium supplemented with 10% FBS in the bottom chamber. The migrated cells were then dissociated from membrane of top chamber and stained with Calcein-AM (Trevigen). The intensity of fluorescence signal in each well was measured using 485 nm/530 nm (excitation/emission) wavelength. Each determination represents the average of three individual wells. Migration/invasion was normalized to percent migration/invasion, with migration/invasion of untreated cells representing 100% migration/invasion.

Superresolution Vutara Imaging. A2780 cells were incubated with FITC-P-Cy5 model conjugate in RPMI-1640 medium for 4, 8, and 12 h at 37 °C at a final concentration of 1 μM. The cells were also stained with 50 nM LysoTracker Red DND-99 for 20 min. After incubation, cells were washed two times with PBS and fixed with 4% (wt/vol) paraformaldehyde. The cell samples were transferred onto glass-bottom microwell dishes (MatTek) and visualized under a 3D Vutara SR-200 fluorescence microscope equipped with a FITC filter (excitation/emission = 488/500–550 nm), a Cy5 filter (excitation/emission = 647/650–720 nm), and a Red DND-99 filter (excitation/emission = 561/580–640 nm) (16). The images were analyzed using SRX software (Vutara).

Tumor Model. All animal studies were carried out in accordance with the University of Utah Institutional Animal Care and Use Committee guidelines under approved protocols. A2780 human ovarian cancer cells (5×10^6) in 100 μL of PBS were subcutaneously inoculated in right flank of 6- to 8-wk-old syngeneic female nude mice (22–25 g; Charles River Laboratories).

Pharmacokinetics and Biodistribution Study. For pharmacokinetic study, 6- to 8-wk-old healthy female nude mice (22–25 g; Charles River Laboratories) ($n = 5$) were intravenously injected with dual-labeled ^{125}I-Tyr-P-DTPA-^{111}In (1 mg, 20 μCi per mouse), and ^{125}I-labeled HPMA copolymer-drug conjugates (P-PTX, P-GEM, 2P-PTX and 2P-GEM) (2 mg, 20 μCi per mouse), respectively. At predetermined intervals, blood samples (10 μL) were taken from the tail vein, and the radioactivity of each sample was measured with Gamma Counter (Packard). According to a previous report (17), ^{125}I activity was counted in a channel with windows set for 15–85 keV and ^{111}In activity was counted in a channel having windows set for 237–257 keV. Cross-counts in the ^{125}I channel were 5% and in the ^{111}In channel were 1.5%. Gross cpm values were corrected to compensate for cross-counting. The blood pharmacokinetic parameters for the radiotracer were analyzed using a noncompartmental model with WinNonlin 5.0.1 software (Pharsight). For biodistribution study, 6- to 8-wk-old female nude mice bearing s.c. A2780 tumors (22–25 g; Charles River Laboratories) ($n = 5$) received intravenous injection of dual-labeled ^{125}I-Tyr-P-DTPA-^{111}In (1 mg, 20 μCi per mouse). At 48 and 96 h after administration, the mice were killed. Various tissues (heart, liver, spleen, kidney, bladder, lung, stomach, intestine, muscle, bone, brain, and tumor) were harvested, weighed, and counted for radioactivity with Gamma Counter (Packard) with the aforementioned ^{111}In/^{125}I dual-isotope protocol. Uptake of the conjugate was calculated as the percentage of the injected dose per gram of tissue (% ID/g). Calculated pharmacokinetic parameters are summarized in Tables S4 and S5.

SPECT/CT Imaging. Dual-labeled model conjugate ^{125}I-Tyr-P-DTPA-^{111}In and ^{125}I-labeled HPMA copolymer-drug

conjugates (2P-PTX, 2P-GEM) were intravenously injected via the tail vein into nude mice bearing subcutaneous A2780 ovarian tumors, respectively (2 mg, 200 μCi per mouse). At 24 and 48 h after administration, mice were anesthetized with 2% (vol/vol) isoflurane gas (IMWI/VetOne) in oxygen and positioned prone on the scanner bed. single-photon emission computed tomography (SPECT)/CT images of mice were acquired by using an Inveon trimodality PET/SPECT/CT scanner (Siemens). A sensor was used to monitor the respiration rate of mice under anesthesia. CT images consisting of 220° and 480 projections at each of two bed positions were acquired first. The exposure time was 135 ms with a detector setting at 80 kVp and 500 μA. Data were reconstructed onto a 416 × 416 × 752 image matrix using the COBRA software package (Exxim). The effective image pixel size was 97 μm. SPECT data were acquired immediately following the CT using a single pinhole collimator with a detector radius of rotation at 35 mm. Images were acquired over 1.5 detector revolutions with 6° between each of 90 projections. A 90-mm bed travel was used. Each projection was acquired for 12 s. The data of ^{125}I images were histogrammed with a window setting of 15–85 keV, and the data of ^{111}In image were histogrammed using a window setting of 149–194 keV. Reconstruction was performed using ordered subset expectation maximization 3D with eight iterations and six subsets. Reconstructed images were analyzed and visualized using the Siemens Inveon Research Workplace software.

In Vivo Antitumor Activity. The antitumor efficacy of combination treatments, including free-drug combination (PTX→GEM) and their conjugates combinations (P-PTX→P-GEM, 2P-PTX→2P-GEM), was evaluated in female nude mice bearing subcutaneous A2780 ovarian tumors. Three weeks after inoculation, when the tumor reached ∼4–5 mm in diameter, mice were randomly assigned to four groups. As shown in Fig. 3*C*, the mice in the drug-treated group received one dose of PTX or HPMA copolymer-PTX conjugates (20 mg/kg PTX equivalent) on day 0 and three doses of GEM or HPMA copolymer-GEM conjugates (5 mg/kg GEM equivalent) on day 1, 7, and 14 through intravenous injection (n = 5). The mice in the control group received saline (n = 5). The day that mice received PTX or its conjugates treatment was set as day 0. The tumor size was measured to monitor the tumor growth. The tumor volume at day 0 was normalized to 100%. All subsequent tumor volumes and body weight were then expressed as the percentage relative to those at day 0. At the end of the experiment, the animals were killed and the tumors were photographed. In addition, the major organs (heart, liver, spleen, lung, kidney, and tumor) of mice were harvested, cryosectioned, and stained for immunohistological analysis.

Immunohistochemistry. After the in vivo treatment study, the slices of major organs (heart, liver, spleen, lung, and kidney) of mice were stained with hematoxylin and eosin (H&E), and examined under a microscope. The slices of tumors treated with saline or combination therapy were immunostained with rabbit polyclonal anti-CD31 antibody (Abcam) and rabbit polyclonal anti-Ki67 antibody (Abcam) using a commercial kit according to the manufacturer's protocol. The slices were examined under a microscope. For TUNEL staining, the slides of tumors treated with saline or combination therapy were stained with ApopTag Plus Fluorescein In-Situ Apoptosis Detection Kit (Life Technologies) according to the manufacturer's instructions. The cellular fluorescence was examined under an Olympus FV1000-XY confocal microscope equipped with 488/510 nm filter for TUNEL staining.

Statistical Analysis. Data were presented as mean ± SD. Statistical analyses were done using a two-tailed unpaired Student t test, with P values of <0.01 indicating statistically significant differences.

SI Discussion

Our second-generation conjugate-mediated combination therapeutics showed superiority, not only over the first-generation conjugate combination, as shown in Fig. 3, but also over the previously reported combination systems against the same ovarian carcinoma. For example, Gallo et al. combined GEM (20 mg/kg) and liposomal doxorubicin (6 mg/kg) to treat A2780 tumor; only 3 of 10 mice were tumor-free at the end of the study (18). Although the majority of mice had a complete tumor regression after increasing doses of two drugs (GEM: 80 mg/kg; liposomal doxorubicin: 15 mg/kg) (18), the total dose of GEM (80 mg/kg, 20 mg/kg) in their experiment was much higher than ours (15 mg/kg = 5 mg/kg × 3). On the other hand, the combination of PTX with other drugs was also tested on the same tumor model. For example, one group treated mice bearing A2780 tumor with the combination of lonafarnib and PTX (20 mg/kg, at days 0, 4, 7, and 11), and the tumors only regressed by 60% (19). In addition, a combination of carboplatin and PTX (10 mg/kg) for two 5-d cycles (20), and a combination of vandetanib and PTX (20 mg/kg) for three 5-d cycles (21) were also evaluated in this tumor model. Unfortunately, all of those studies did not achieve complete tumor regression at the end of the trial. Apparently, our second-generation conjugate combination showed overwhelming success against A2780 ovarian carcinoma: two mice were tumor-free and the other three mice had tumor at ∼3% of initial size. If those three mice with tiny tumor were given extra dose of PTX or GEM conjugate, they might have been totally cured.

Another advantage of our PTX and GEM conjugates combination is their potential to overcome drug resistance. Overexpression of PgP (P-glycoprotein) and multidrug resistance-associated protein is a key factor contributing to the development of multidrug resistance in cancer cells and leading to the failure of many forms of chemotherapy in current clinics. According to the findings by Bergman et al., PgP- and multidrug resistance-associated protein-overexpressing cells are more sensitive to gemcitabine than their parental cells (22). The increased sensitivity is related to deoxycytidine kinase and gemcitabine effects on DNA. Thus, the cancer cells, which have PgP-mediated PTX resistance, might show increased sensitivity to GEM. In addition, our drug delivery system releases drug molecules intracellularly and avoids the membrane efflux pumps, like PgP. So the combination of GEM and PTX conjugates in our system is able to kill drug-sensitive cells as well as drug-resistant cancer cells.

Such success is attributed to enhanced bioavailability, prolonged circulation time, increased intratumoral drug concentration, and combination strategy. The prerequisite for all those improvements is incorporation of cathepsin B-sensitive linker GFLG in our delivery system. The cysteine proteinase, cathepsin B, normally locates in the cellular lysosomes and contributes to degradation and regulation of proteins (23). However, in malignant tumors, such as melanoma (24), breast (25), ovarian (26, 27), lung (28), stomach (29), and colon (30) tumors, cathepsin B is secreted extracellularly and acts as an important proteinase of matrix materials to degrade surrounding proteins and other tissue components so that cancer cells can invade and metastasize. It has been reported that cathepsin B level is much higher in malignant ovarian tumor than in normal ovary tissues (26) and its expression is regarded as a marker for ovarian cancer prognosis (31). In our design, the second-generation enzyme-responsive carriers can release PTX and GEM in the same organ, tissue, or cells with a high level of cathepsin B, like ovarian tumors, so as to enhance the uptake ratio of tumor-to-nontumor. In summary, the controlled release property of our polymeric carriers can normalize the pharmacokinetics, biodistribution, and stability of chemically dissimilar drugs that have disparate pharmacological behavior, which allow synergistic dosing over a longer duration of treatment compared with the free drugs.

1. Mitsukami Y, Donovan MS, Lowe A, Mccormick CL (2001) Water-soluble Polymers. 81. Direct synthesis of hydrophilic styrenic-based homopolymers and block copolymers in aqueous solution via RAFT. *Macromolecules* 34(7):2248–2256.
2. Pan H, Yang J, Kopečková P, Kopeček J (2011) Backbone degradable multiblock *N*-(2-hydroxypropyl)methacrylamide copolymer conjugates via reversible addition-fragmentation chain transfer polymerization and thiol-ene coupling reaction. *Biomacromolecules* 12(1):247–252.
3. Kopeček J, Bažilová H (1973) Poly[*N*-(2-Hydroxypropyl)methacrylamide]. 1. Radical polymerization and copolymerization. *Eur Polym J* 9(1):7–14.
4. Kopeček J, et al. (1991) Synthetic polymeric drugs. US Patent 5,037,883.
5. Duncan R, Cable HC, Rejmanová P, Kopeček J, Lloyd JB (1984) Tyrosinamide residues enhance pinocytic capture of *N*-(2-hydroxypropyl)methacrylamide copolymers. *Biochim Biophys Acta* 799(1):1–8.
6. Omelyanenko V, Kopečková P, Gentry C, Kopeček J (1998) Targetable HPMA copolymer-adriamycin conjugates. Recognition, internalization, and subcellular fate. *J Control Release* 53(1-3):25–37.
7. Šubr V, Ulbrich K (2006) Synthesis and properties of new N-(2-hydroxypropyl) methacrylamide copolymers containing thiazolidine-2-thione reactive groups. *React Funct Polym* 66(12):1525–1538.
8. Zhang R, et al. (2013) Synthesis and evaluation of a backbone biodegradable multiblock HPMA copolymer nanocarrier for the systemic delivery of paclitaxel. *J Control Release* 166(1):66–74.
9. Yang J, Luo K, Pan H, Kopečková P, Kopeček J (2011) Synthesis of biodegradable multiblock copolymers by click coupling of RAFT-generated heterotelechelic polyHPMA conjugates. *React Funct Polym* 71(3):294–302.
10. Larson N, et al. (2013) Biodegradable multiblock poly(*N*-2-hydroxypropyl)methacrylamide gemcitabine and paclitaxel conjugates for ovarian cancer cell combination treatment. *Int J Pharm* 454(1):435–443.
11. Starcher B (2001) A ninhydrin-based assay to quantitate the total protein content of tissue samples. *Anal Biochem* 292(1):125–129.
12. Merkel OM, et al. (2009) In vivo SPECT and real-time gamma camera imaging of biodistribution and pharmacokinetics of siRNA delivery using an optimized radiolabeling and purification procedure. *Bioconjug Chem* 20(1):174–182.
13. Pippin CG, Parker TA, McMurry TJ, Brechbiel MW (1992) Spectrophotometric method for the determination of a bifunctional DTPA ligand in DTPA-monoclonal antibody conjugates. *Bioconjug Chem* 3(4):342–345.
14. Chou TC, Motzer RJ, Tong Y, Bosl GJ (1994) Computerized quantitation of synergism and antagonism of taxol, topotecan, and cisplatin against human teratocarcinoma cell growth: A rational approach to clinical protocol design. *J Natl Cancer Inst* 86(20): 1517–1524.
15. Chou TC, Talalay P (1984) Quantitative analysis of dose-effect relationships: The combined effects of multiple drugs or enzyme inhibitors. *Adv Enzyme Regul* 22:27–55.
16. Juette MF, et al. (2008) Three-dimensional sub-100 nm resolution fluorescence microscopy of thick samples. *Nat Methods* 5(6):527–529.
17. Carney PL, Rogers PE, Johnson DK (1989) Dual isotope study of iodine-125 and indium-111-labeled antibody in athymic mice. *J Nucl Med* 30(3):374–384.
18. Gallo D, et al. (2006) Preclinical in vivo activity of a combination gemcitabine/liposomal doxorubicin against cisplatin-resistant human ovarian cancer (A2780/CDDP). *Int J Gynecol Cancer* 16(1):222–230.
19. Taylor SA, et al. (2008) Combining the farnesyltransferase inhibitor lonafarnib with paclitaxel results in enhanced growth inhibitory effects on human ovarian cancer models in vitro and in vivo. *Gynecol Oncol* 109(1):97–106.
20. Munk Jensen M, et al. (2013) Imaging of treatment response to the combination of carboplatin and paclitaxel in human ovarian cancer xenograft tumors in mice using FDG and FLT PET. *PLoS ONE* 8(12):e85126.
21. Cesca M, et al. (2009) The effects of vandetanib on paclitaxel tumor distribution and antitumor activity in a xenograft model of human ovarian carcinoma. *Neoplasia* 11(11):1155–1164.
22. Bergman AM, et al. (2003) Increased sensitivity to gemcitabine of P-glycoprotein and multidrug resistance-associated protein-overexpressing human cancer cell lines. *Br J Cancer* 88(12):1963–1970.
23. Sloane BF (1990) Cathepsin B and cystatins: Evidence for a role in cancer progression. *Semin Cancer Biol* 1(2):137–152.
24. Sloane BF, Dunn JR, Honn KV (1981) Lysosomal cathepsin B: Correlation with metastatic potential. *Science* 212(4499):1151–1153.
25. Lah TT, et al. (1995) Cathepsins D, B and L in breast carcinoma and in transformed human breast epithelial cells (HBEC). *Biol Chem Hoppe Seyler* 376(6):357–363.
26. Downs LS, Jr, Lima PH, Bliss RL, Blomquist CH (2005) Cathepsins B and D activity and activity ratios in normal ovaries, benign ovarian neoplasms, and epithelial ovarian cancer. *J Soc Gynecol Investig* 12(7):539–544.
27. Nishikawa H, et al. (2004) The role of cathepsin B and cystatin C in the mechanisms of invasion by ovarian cancer. *Gynecol Oncol* 92(3):881–886.
28. Ebert W, et al. (1994) Prognostic value of increased lung tumor tissue cathepsin B. *Anticancer Res* 14(3A):895–899.
29. Chung SM, Kawai K (1990) Protease activities in gastric cancer tissues. *Clin Chim Acta* 189(2):205–210.
30. Adenis A, et al. (1995) Cathepsin B, L, and D activities in colorectal carcinomas: Relationship with clinico-pathological parameters. *Cancer Lett* 96(2):267–275.
31. Scorilas A, et al. (2002) Determination of cathepsin B expression may offer additional prognostic information for ovarian cancer patients. *Biol Chem* 383(7-8):1297–1303.

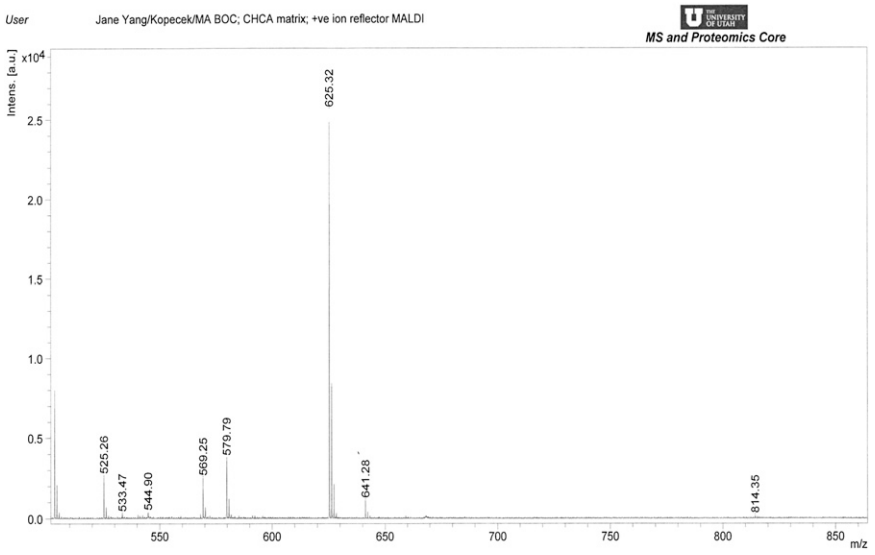

Fig. S1. MALDI-TOF mass spectrum of 2-(*N*-methacryloylglycylphenylalanylleucylglycine)-*N*′-Boc-ethylenediamine (MA-GFLG-NH-Boc).

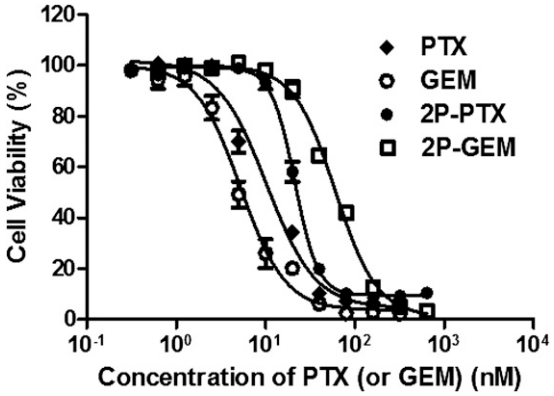

Fig. S2. In vitro cytotoxicity of free drugs (PTX, GEM) and their HPMA conjugates (2P-PTX, 2P-GEM) toward A2780 human ovarian carcinoma cells.

A

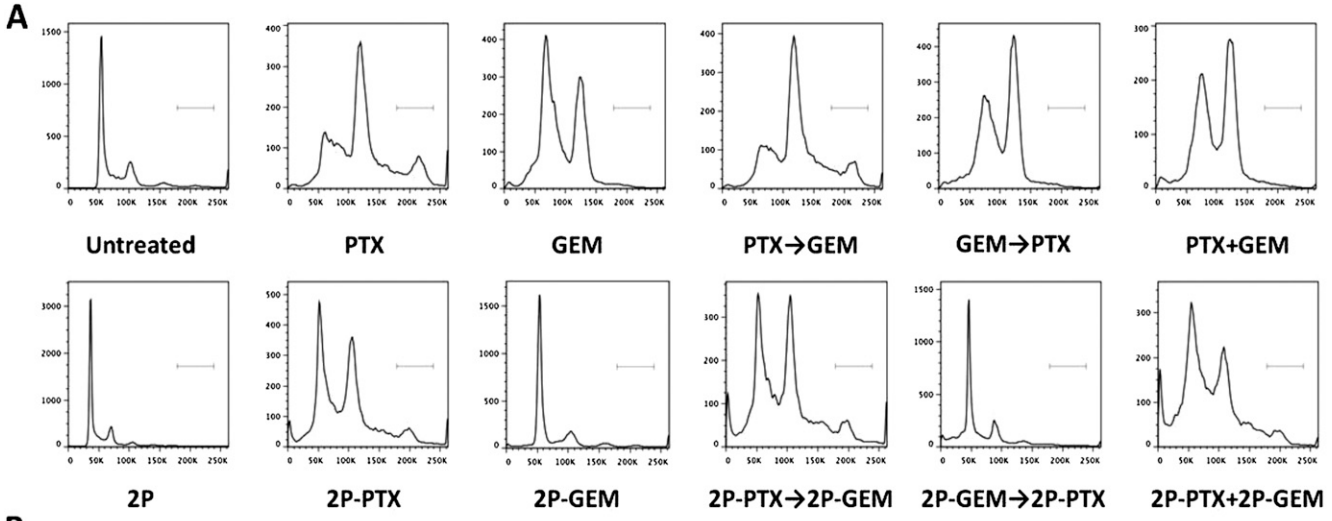

B

Treatment	% G_0/G_1	% S	% G_2/M	% Hyper G_2/M
Untreated	45.5 ±7.2	26.8±2.6	15.2±2.4	4.4±0.9
PTX	14.0±1.6	23.3±0.9	34.8±2.8	14.2±0.6
GEM	34.5±1.4	31.0±1.0	24.6±1.2	1.9±0.2
PTX→GEM	12.8±1.3	26.3±5.4	32.3±4.7	13.9±0.9
GEM→PTX	29.4±0.7	35.1±5.2	33.1±6.7	1.9±0.2
PTX + GEM	31.8±1.1	31.0±4.4	36.1±6.5	2.5±0.3
2P	49.4±1.9	21.9±2.6	15.9±0.8	1.6±0.4
2P-PTX	19.6±1.2	25.6±1.2	21.7±1.9	7.3±0.7
2P-GEM	49.2±5.3	27.1±2.4	16.0±0.8	4.4±0.5
2P-PTX→2P-GEM	19.1±0.2	23.9±0.5	27.4±2.6	8.1±0.1
2P-GEM→2P-PTX	43.4±4.1	21.1±1.5	14.5±1.5	3.1±0.4
2P-PTX + 2P-GEM	33.3±0.7	22.9±1.3	19.8±0.3	5.1±0.2

Fig. S3. Effect of treatment with PTX, GEM, or their combinations on cell cycle. A2780 cells were treated with drug alone (PTX, GEM), conjugate alone (2P-PTX, 2P-GEM) or their different sequential combinations. Cell cycle analysis was performed by flow cytometry after propidium iodide staining. (*A*) The representative DNA histograms of cells after treatments are shown. (*B*) Cell cycle distribution in A2780 cells after treatments are presented as mean ± SD ($n = 3$).

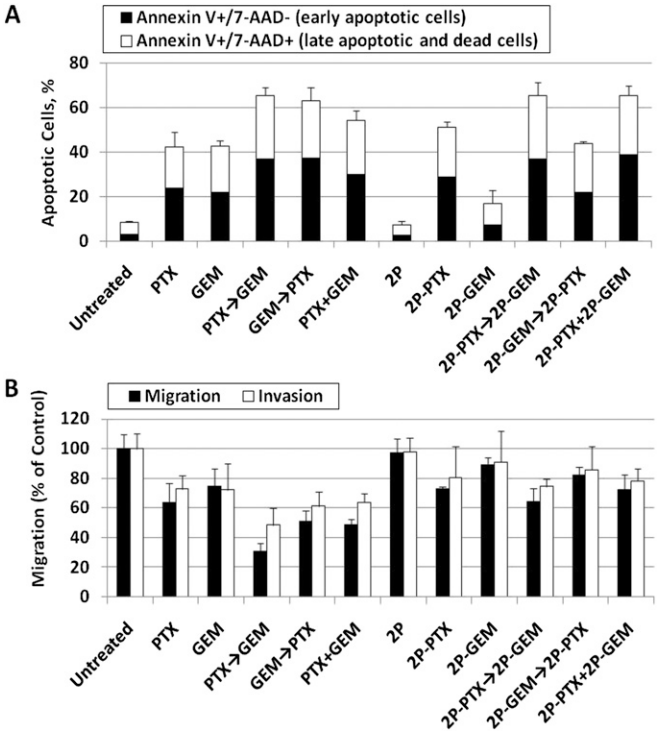

Fig. S4. Treatment with PTX followed by GEM in vitro showed superior antitumor potency. (*A*) Annexin V/7-AAD apoptosis analysis in A2780 cells after single treatment or different sequential combinations. (*B*) Inhibition of cell migration and invasion by single treatment or different sequential combinations in A2780 cells. Migration was normalized to percent migration with 100% representing migration of untreated cells. The final concentration of drugs in single and combination treatments: PTX = 10 nM, GEM = 10 nM, 2P-PTX = 20 nM, and 2P-GEM = 20 nM. All of the data are expressed as mean ± SD (n = 3–4).

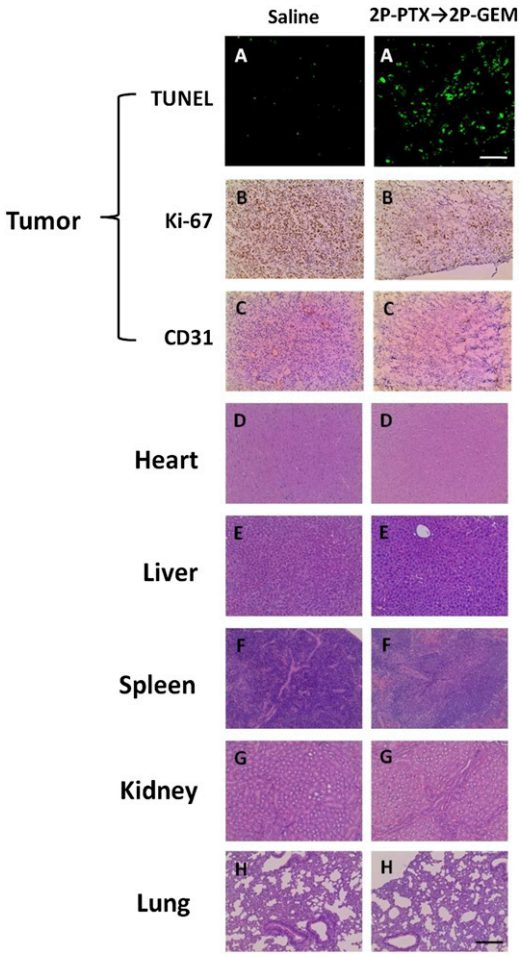

Fig. S5. Immunohistochemical analysis of tumors and major organs from tumor-bearing mice treated with saline (control) or combination of second generation conjugates. The tissues (tumor, heart, liver, spleen, kidney, and lung) were sliced with 5-μm thickness. The tumor sections were stained with TUNEL (*A*), K_i-67 (*B*), and CD31 (*C*) for antitumor evaluation. (*D*–*H*) The sections of major organs were stained with H&E for safety evaluation. (Scale bar, 100 μm.)

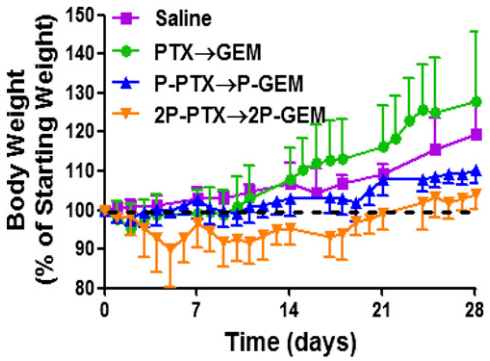

Fig. S6. Body weight change in mice treated with saline, free-drug combination (PTX→GEM), and their conjugate combinations (P-PTX→P-GEM, 2P-PTX→2P-GEM). The data are presented as mean ± SD (n = 4–5).

Table S1. Summary of conjugates

Application	Conjugate	Mw (kDa)	Mw/Mn	Drug% (wt)
In vivo treatment	P-GEM	40	1.07	8.2
	2P-GEM	110	1.12	10.1
	P-PTX	50	1.08	7.2
	2P-PTX	115	1.34	7.9
Pharmacokinetics and biodistribution	P-GEM-Tyr	32	1.05	8.2
	2P-GEM-Tyr	89	1.07	8.5
	P-PTX-Tyr	48	1.05	7.3
	2P-PTX-Tyr	113	1.29	7.9
Model conjugates	^{111}In-P-^{125}I	35	1.12	N/A
	^{111}In-2P-^{125}I	93	1.13	N/A
	FITC-P-Cy5	50	1.07	N/A

Table S2. Treatment groups

Group	Treatment
Untreated	Medium w/o drug (72 h)
2P	2P (48 h) → medium w/o drug (24 h)
PTX	PTX (24 h) → medium w/o drug (48 h)
GEM	GEM (24 h) → medium w/o drug (48 h)
PTX→GEM	PTX (24 h) → GEM (24 h) → medium w/o drug (24 h)
GEM→PTX	GEM (24 h) → PTX (24 h) → medium w/o drug (24 h)
PTX + GEM	PTX and GEM (24 h) → medium w/o drug (48 h)
2P-PTX	2P-PTX (24 h) → medium w/o drug (48 h)
2P-GEM	2P-GEM (24 h) → medium w/o drug (48 h)
2P-PTX→2P-GEM	2P-PTX (24 h) → 2P-GEM (24 h) → medium w/o drug (24 h)
2P-GEM→2P-PTX	2P-GEM (24 h) → 2P-PTX (24 h) → medium w/o drug (24 h)
2P-PTX + 2P-GEM	2P-PTX and 2P-GEM (24 h) → medium w/o drug (48 h)

2P, diblock HPMA copolymer; 2P-PTX, diblock HPMA copolymer-paclitaxel conjugate; 2P-GEM, diblock HPMA copolymer-gemcitabine conjugate; w/o = without.

Table S3. CI values of different sequential combination treatments in A2780 cells

	Combination index			
Treatment	Fa_{25}	Fa_{50}	Fa_{75}	Fa_{90}
PTX→GEM	0.51 ± 0.07	0.41 ± 0.05	0.34 ± 0.05	0.28 ± 0.05
GEM→PTX	0.76 ± 0.18	0.73 ± 0.10	0.70 ± 0.04	0.68 ± 0.05
PTX + GEM	1.23 ± 0.22	1.19 ± 0.11	1.15 ± 0.02	1.13 ± 0.08
2P-PTX→2P-GEM	0.38 ± 0.07	0.55 ± 0.06	0.81 ± 0.01	1.18 ± 0.09
2P-GEM→2P-PTX	1.48 ± 0.22	1.51 ± 0.18	1.54 ± 0.14	1.58 ± 0.10
2P-PTX + 2P-GEM	0.46 ± 0.06	0.70 ± 0.06	1.06 ± 0.05	1.62 ± 0.03

Table S4. Comparison of pharmacokinetic parameters for ^{125}I-labeled conjugates in mice

Parameter	P-PTX	2P-PTX	P-GEM	2P-GEM
$T_{1/2,\alpha}$ (h)	0.88 ± 0.11	1.13 ± 0.13 *	0.26 ± 0.02	1.45 ± 0.36 ***
$T_{1/2,\beta}$ (h)	13.30 ± 1.28	37.90 ± 3.55 ***	6.36 ± 0.66	32.07 ± 2.50 ***
AUC (%ID h/mL blood)	420.95 ± 26.05	1206.42 ± 85.97 ***	108.66 ± 6.74	1481.23 ± 83.06 ***
CL (mL/h)	0.24 ± 0.01	0.08 ± 0.01 ***	0.92 ± 0.06	0.07 ± 0.004 ***
MRT (h)	18.25 ± 1.71	52.86 ± 4.95 ***	8.49 ± 0.88	45.39 ± 3.43 ***
Vss (mL)	4.34 ± 0.16	4.38 ± 0.16	7.82 ± 0.38	3.06 ± 0.10 ***

AUC, total area under the blood concentration versus time curve; %ID, percentage of injected dose; CL, total body clearance; MRT, mean residence time; $T_{1/2,\alpha}$, initial half-life; $T_{1/2,\beta}$, terminal half-life; Vss, steady-state volume of distribution. Data are presented as mean ± SD ($n = 5$). *$P < 0.01$, ***$P < 0.001$.

Table S5. Comparison of pharmacokinetic parameters for ^{111}In-DTPA and ^{125}I-Tyr-P in mice

Parameter	^{111}In-DTPA	^{125}I-Tyr-P
$T_{1/2,\alpha}$ (h)	1.85 ± 0.33	3.02 ± 0.81
$T_{1/2,\beta}$ (h)	27.96 ± 3.05	30.68 ± 5.02
AUC (%ID h/mL blood)	1313.14 ± 89.51	1148.72 ± 99.68
CL (mL/h)	0.08 ± 0.01	0.09 ± 0.01
MRT (h)	38.54 ± 4.02	41.68 ± 6.22
Vss (mL)	2.94 ± 0.14	3.63 ± 0.29

AUC, total area under the blood concentration versus time curve; %ID, percentage of injected dose; CL, total body clearance; MRT, mean residence time; $T_{1/2,\alpha}$, initial half-life; $T_{1/2,\beta}$, terminal half-life; Vss, steady-state volume of distribution. Data are presented as mean ± SD (n = 5).